Instabilities and Mixing in Type II-P and II-b Supernovae

By T. SHIGEYAMA,[1] K. IWAMOTO,[1] I. HACHISU,[1] K. NOMOTO,[1] AND H. SAIO[2]

[1]University of Tokyo, Bunkyo-ku, Tokyo 113, Japan

[2]Tohoku University, Sendai 980, Japan

We calculate a nonlinear growth of the Rayleigh-Taylor instability in the exploding red supergiant stars with a two-dimensional hydrodynamical code, and examine how the extent of mixing depends on the progenitor's core mass and the envelope mass. The results are compared with the observations of type II-P supernovae and the recent type II-b supernova 1993J.

1. Introduction

Large scale mixing in supernova ejecta has been indicated in spectroscopic and photometric observations of various types of supernovae. This has stimulated 2D and 3D hydrodynamical calculations of the Rayleigh-Taylor (R-T) instabilities during supernova explosions for SN 1987A (Arnett *et al.* 1989; Hachisu *et al.* 1990, 1992; Fryxell *et al.* 1991; Müller *et al.* 1991; Den *et al.* 1990; Yamada *et al.* 1990; Yamada & Sato 1991; Herant & Benz 1991, 1992), type Ib/Ic supernovae (Hachisu *et al.* 1991, 1994a), type II-P supernovae (Herant & Woosley 1994; Hachisu *et al.* 1994b), and the type II-b supernova 1993J (Iwamoto *et al.* 1994). In particular, Hachisu *et al.* (1991, 1994a) found that development of the R-T instabilities depend sensitively on the presupernova structure, so that the comparison between hydrodynamical simulations and observations can provide a new clue to the understanding of supernova progenitors, their structure, and the explosion mechanism.

In the present paper, we follow a nonlinear growth of the R-T instabilities in the exploding red supergiant stars, i.e., type II-P and II-b supernovae. We find that the extent of mixing depends on the core mass and the envelope mass of red supergiants.

2. Initial Models

We adopt the red-supergiant progenitor models for type II-P and II-b supernovae (Nomoto & Hashimoto 1988; Saio *et al.* 1988). Their main-sequence masses $M_{\rm ms}$, and their presupernova helium core masses $M_{\rm He}$, H-rich envelope masses $M_{\rm H}$, and the radii R at the explosions are summarized in table 1. The assumed neutron star baryonic masses $M_{\rm NS}$ are also given, so that the ejected H-free core masses are given by $M_{\rm He} - M_{\rm NS}$.

For *type II-P models*, no mass loss is assumed. The core of IIP20 progenitor model is the same as adopted for the model of SN 1987A except for the hydrogen-rich envelope (Shigeyama & Nomoto 1990).

For *type II-b models*, large amount of mass loss is assumed so that almost all hydrogen-rich envelopes are lost at presupernova stage (e.g., Nomoto *et al.* 1993; Shigeyama *et al.* 1994).

https://doi.org/10.1017/S0252921100007995 Published online by Cambridge University Press

TABLE 1. Progenitor models of type II-P and II-b supernovae

Model	$M_{\rm ms}/M_\odot$	$M_{\rm H}/M_\odot$	$M_{\rm He}/M_\odot$	$M_{\rm NS}/M_\odot$	$R/R_\odot$
IIP13	13	9.7	3.3	1.2	360
IIP20	20	14	6	1.6	900
IIb3H11	13	0.11	3.3	1.2	450
IIb4H13	15	0.13	4	1.3	580

3. Rayleigh-Taylor Instabilities and Mixing

A shock wave is generated by depositing thermal energy at the mass cut that divides the ejecta and the neutron star. The final kinetic energy of explosion is assumed to be $E = 1 \times 10^{51}$ erg for all the models. The early phase of shock propagation up to the He/C+O interface is calculated with a spherically symmetric Lagrangian code (Shigeyama & Nomoto 1990). When the blast shock arrives at the bottom of the helium layer, the density, velocity, energy etc. are mapped onto our 2-D grids. Just after the mapping, we perturb only the velocity field all over the mesh points; i.e, the velocity field inside the shock front is perturbed but the velocities outside the shock remain zero.

We assume a random perturbation mode as in Hachisu *et al.* (1992). The amplitude of the perturbation is 5% of the expansion velocity. The mode of random perturbation is $n = 128$ (i.e., the azimuthal angle is divided into 128 and the velocity is perturbed randomly at each divided azimuthal angle). The basic part of our code is based on Chakravarthy & Osher's (1985) third-order accurate, TVD (Total Variation Diminishing) method (Hachisu *et al.* 1992).

3.1. *Type II-P Supernovae*

When the shock wave arrives at the composition interface, the expansion of the core is decelerated to generate a reverse shock. Such a deceleration induces the R-T instabilities which lead to mixing of materials. The nonlinear growth of the R-T instabilities for type II-P supernova explosions is shown in the density contours (left), which is linearly spaced by 5% of the maximum density, and the position of marker particles (right) in Figure 1. Marker particles, which are initially placed at each composition interface, follow the deformation of each composition interface, H/He, He/C+O, and O/Si+Ni. The elemental mixing in these type II-P models are plotted in Figure 2. It is found that the mixing of ^{56}Ni depends on the stellar mass, being substantial for the $\sim 13 M_\odot$ star, but much less for the 20 $M_\odot$ star.

Model IIP20: The R-T instability is weak at the He/C+O interface as found in the model for SN 1987A (Hachisu *et al.* 1990, 1992), but it grows at the H/He interface. The development of R-T instabilities in this II-P model is somewhat different from SN 1987A. Because of the lower envelope density and thus the larger density contrast at the H/He interface, the instability grows faster and mix hydrogen well into the core material at the expansion velocity of as low as 1000 km s^{-1} (Figure 2a). The instability is so strong that the hydrogen, helium, and carbon-oxygen are well mixed even for a small amplitude of 1% and 0.2%.

On the other hand, the propagation of the reverse shock is slower than in SN 1987A due to the lower envelope density. When the blast shock breaks out of the surface ($t \sim 3 \times 10^5$

https://doi.org/10.1017/S0252921100007995 Published online by Cambridge University Press

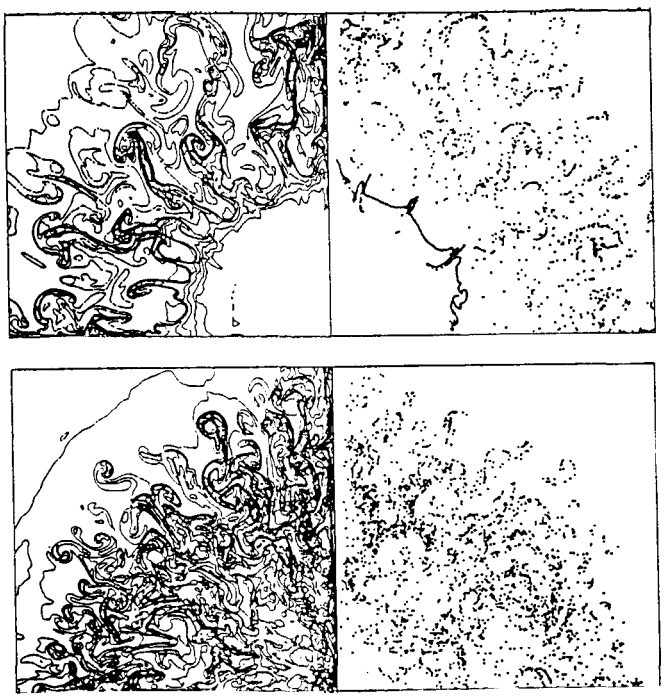

FIGURE 1. Density contour (left) and positions of marker particles (right) on 1025 × 1025 grids for type II-P supernova explosions. (a) *IIP20 (upper)*: Time after the explosion is 8×10^5 s. The size of the computational box is 1.65×10^{14} cm (2400 $R_\odot$). (b) *IIP13 (lower)*: Time after the explosion is 3×10^5 s. The size is 6.8×10^{13} cm (980 $R_\odot$).

s), the reverse shock just arrives at the Si/Ni layer. After the shock breakout, the R-T instability disappears quickly because a rarefaction wave causes the pressure inversion to disappear. Accordingly, the time is too short for the R-T instability to mix the innermost part of the ejecta, i.e., ^{56}Ni is not well mixed as seen from the marker particles at the O/Si+Ni interface (Fig. 1), which is a clear contrast to the model of SN 1987A.

Model IIP13: The R-T instability first grows at the He/C+O interface and then is amplified at the H/He interface. Accordingly ^{56}Ni is well mixed into the middle of the hydrogen-rich envelope. Hydrogen is also well mixed down into the core. The elemental mixing is plotted in Figure 2b. Nickel is mixed up to the layer having the expansion velocity of 2000 km s^{-1} while hydrogen is mixed down to 500 km s^{-1}.

3.2. *SN 1993J*

Figure 3 shows developments of the R-T instabilities as in Figure 1. For both models of 3H11 and 4H13, the R-T instability first grows at the He/C+O interface as in IIP13. For the smaller mass core, the instability is stronger because of larger deceleration due to larger mass ratio between the He-layer and the heavy element layer (Hachisu *et al.* 1991). The instabilities induce mixing of heavy elements (including ^{56}Ni) into the helium layer. The extent of ^{56}Ni mixing is larger for the smaller mass helium core. It also depends on the degree of premixing of ^{56}Ni due to the R-T instability induced by neutrino heating (Herant *et al.* 1992). The R-T instability at the H/He interface also grows because of the large density jump across the core and the low density envelope. The instability is

https://doi.org/10.1017/S0252921100007995 Published online by Cambridge University Press

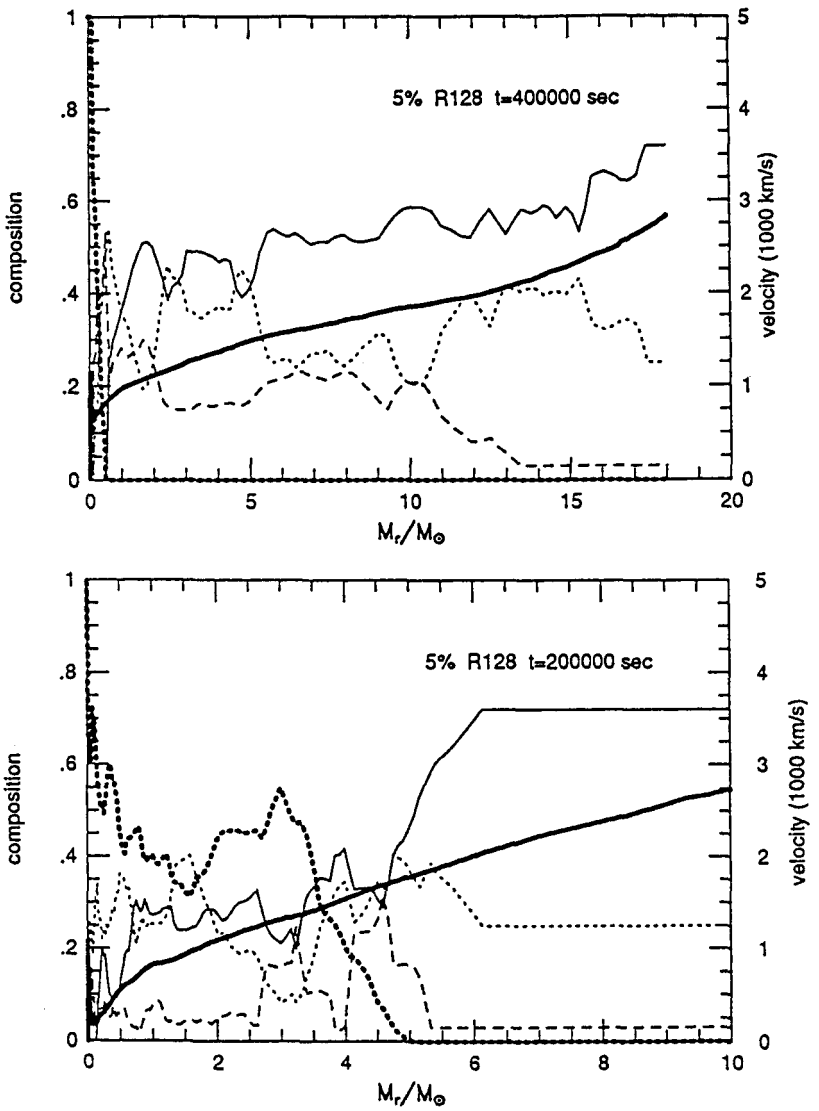

FIGURE 2. Elemental abundances are averaged along the angular direction and plotted against the mass coordinate, M_r, for the models in Figure 1. Shown are H (thin solid), He (short-dashed), C+O (long-dashed), and Si+^{56}Ni (thick-dashed). The averaged expansion velocity (thick solid) is also shown. (a) *IIP20 (upper)*: Ni+Si are localized near the center but hydrogen is well mixed into the core having an expansion velocity of 1000 km s^{-1}. (b) *IIP13 (lower)*: Ni+Si are well mixed into the hydrogen-rich envelope. Conversely hydrogen is mixed down to the layer having an expansion velocity of 500 km s^{-1}.

weaker than in type II-P supernova models and SN 1987A because the deceleration of the core expansion is weaker due to the much smaller envelope mass. However, a certain degree of mixing between the H-rich envelope and the helium layer is found.

Figure 4 shows the abundance distribution of H, He, C+O, and Si+Ni for 3H11 in 2D and 1D calculations (i.e., with and without mixing) against the expansion velocity. Oxygen and ^{56}Ni are mixed up to the expansion velocity of 6000 km s^{-1} and 5300 km s^{-1}, respectively.

https://doi.org/10.1017/S0252921100007995 Published online by Cambridge University Press

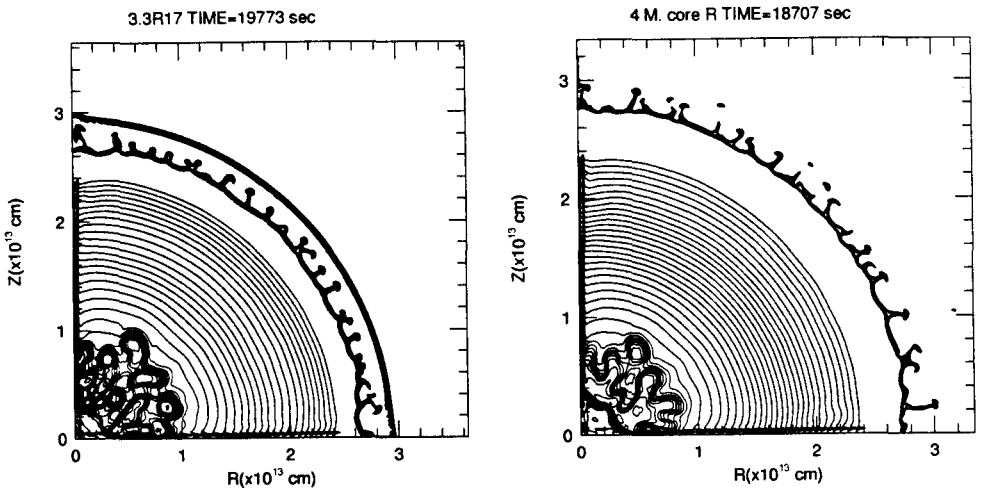

FIGURE 3. Developments of Rayleigh-Taylor instabilities in the models for the type II-b supernova SN 1993J: 4H13 (right) and 3H11 (left). Instabilities at both interfaces of H/He and He/C+O are observed.

4. Comparison with Observations

Light curves of type II-P supernovae are characterized by the plateau which last typically $\sim$ 100 day. The shape of the light curve is determined by the receding hydrogen recombination front in the ejecta (Grasberg *et al.* 1971). The plateau phase is longer as the minimum expansion velocity of hydrogen is lower, i.e., the mass of H-rich envelope is larger and/or the mixing of hydrogen into the low velocity core is deeper (Shigeyama & Nomoto 1990). Therefore, the length of the plateau may provide an indication of mixing as is the case of SN 1987A.

The mixing of ^{56}Ni also affect the light curve due to radioactive heating. Its extent is different between the above two progenitors: ^{56}Ni is mixed up to the middle of the hydrogen-rich envelope in the 13 $M_\odot$, while it is hardly mixed for the 20 $M_\odot$ stars.

The light curve of SN 1993J can be better reproduced with the above models if some ^{56}Ni is mixed into the helium layer. The extent of ^{56}Ni mixing found in these models is consistent with that suggested from the light curve. The small extent of hydrogen mixing is consistent with the relatively high hydrogen velocity in SN 1993J.

More direct indication of mixing in SN 1993J has been provided by the emission line features of oxygen (Wang & Hu 1993; Spyromilio 1993) which indicate the presence of clumps. Since the instabilities at the He/C+O interface grows only for $M_{\rm ms}$ = 13 – 15 $M_\odot$ but not for $M_{\rm ms} \sim 20 M_\odot$, such clumps in SN 1993J are consistent with the progenitor mass of $M_{\rm ms}$ = 13 – 15 $M_\odot$ as estimated from the light curve (Nomoto *et al.* 1993; Wheeler & Filippenko 1994).

Acknowledgements

This work has been supported in part by the Grant-in-Aid for Scientific Research (04640265, 05242102, 05242103, 05242207) of the Japanese Ministry of Education, Science, and Culture, KEK, the Space Data Analysis Center of ISAS, and K*i*CFD.

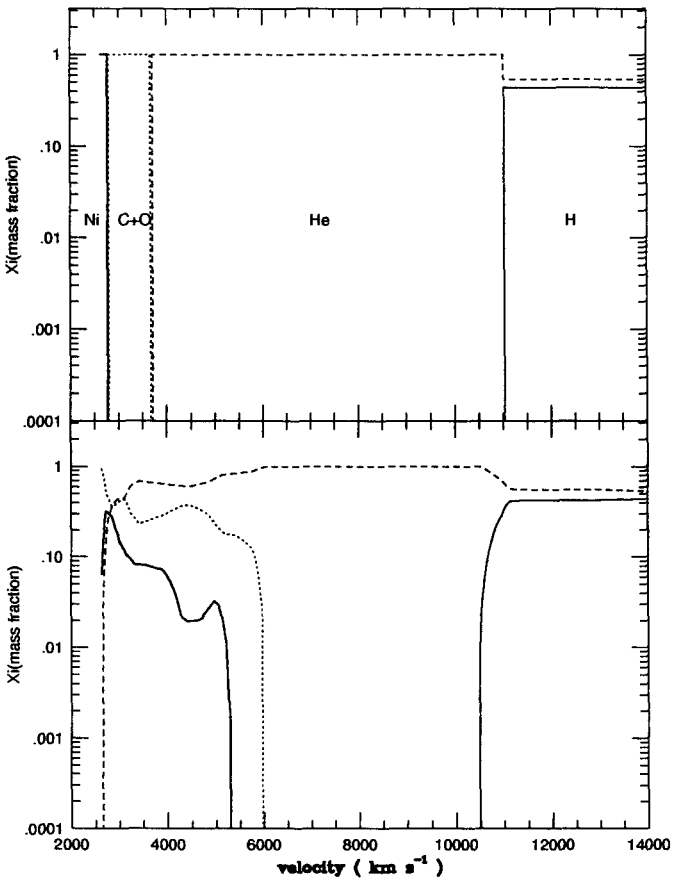

FIGURE 4. The abundance distribution of H, He, C+O, and Si+Ni for 3H11 in 1D and 2D calculations (i.e., with and without the mixing) against the expansion velocity.

REFERENCES

Arnett W.D., Fryxell B.A., & Müller E. 1989, ApJ, 341, L63
Chakravarthy S.R., & Osher S. 1985, AIAA Paper No. 85-0363
Den M., Yoshida T., & Yamada Y. 1990, Progr. Theor. Phys., 83, 723
Fryxell B.A., Müller E., & Arnett W.D. 1991, ApJ, 367, 619
Grasberg E.K., Imshennik, V.S., Nadezhin, D.K. 1971, Ap.Space Sci., 10, 28
Hachisu I., Matsuda T., Nomoto K., & Shigeyama T. 1990, ApJ, 358, L57
Hachisu I., Matsuda T., Nomoto K., & Shigeyama T. 1991, ApJ, 368, L27
Hachisu I., Matsuda T., Nomoto K., & Shigeyama T. 1992, ApJ, 390, 230
Hachisu I., Matsuda T., Nomoto K., & Shigeyama T. 1994a, A&AS, in press
Hachisu, I., Nomoto, K., & Shigeyama, T. 1994b, in ApJ, 390, 230
Herant M., & Benz W. 1991, ApJ, 370, L81
Herant M., & Benz W. 1992, ApJ, 387, 294
Herant M., Benz W. , & Colgate, S. A. 1992, ApJ 395, 642
Herant M., & Woosley, S.E. 1994, ApJ, 425, 814
Iwamoto, K., Hachisu, I., Shigeyama, T., & Nomoto, K. 1994, in preparation
Müller E., Fryxell B., & Arnett W.D. 1991, A&A, 251, 505

https://doi.org/10.1017/S0252921100007995 Published online by Cambridge University Press

Nomoto, K., & Hashimoto, M. 1988, Phys. Rep. 163, 13

Nomoto K., Shigeyama T., Kumagai S., Yamaoka H., & Suzuki T 1993, in: Supernovae (Les Houches, Session LIV), ed. J. Audouze *et al.* , Elsevier Sci. Publ., in press

Nomoto, K., Suzuki, T., Shigeyama, T., Kumagai, S., Yamaoka, H., & Saio, H. 1993, Nature, 364, 507

Saio, H., Nomoto, K., & Kato, M. 1988, Nature ,334, 508

Shigeyama, T., & Nomoto, K. 1990, ApJ, 360, 242

Shigeyama, T., Nomoto, K., Tsujimoto, T & Hashimoto, M. 1990, ApJ, 361, L23

Shigeyama, T., Suzuki, T., Kumagai, S., Nomoto, K., Saio, H., & Yamaoka, H. 1994, ApJ, 420, 341

Wheeler, J.C., & Filippenko, A.V. 1993, in this volume

Yamada Y., Nakamura T., & Oohara K. 1990, Progr. Theor. Phys., 84, 436

Yamada S., & Sato K. 1991, ApJ, 382, 594